

# Diagnosis and differential diagnosis of cerebral fat embolism

PhD THESIS

**Omar Giyab MD**

Doctoral School of Clinical Neurosciences

Clinical and Human Neurosciences Program

Supervisors:

Arnold Tóth, MD, PhD and Gergely Orsi, PhD

Program Leader: Prof. József Janszky, MD, PhD

Doctoral School Leader: Prof. Sámuel Komoly, MD, PhD



Department of Medical Imaging

University of Pécs, Medical School

Pécs, 2023

## 1. Introduction

Fat embolism (FE) is a pathophysiological phenomenon and must be differentiated from fat embolism syndrome (FES), which is defined by the presence of clinical signs and symptoms resulting from embolic showers. Cerebral fat embolism (CFE) denotes the embolization of fat particles to the brain and is the focus of this work. FE, FES, and CFE all share a similar pathophysiologic background. CFE is part of the FES, which is the consequence of the intravascular embolisation of fat globules. The most common cause of FES is displaced long bone fractures, or during orthopaedic procedures but it may also be induced by other conditions as well. CFE was first described by Zenker in 1862, but to this day its exact pathophysiology remains poorly understood. Both mechanical and biochemical theories have been proposed to explain the syndrome. The most likely mechanism of tissue injury is the mechanical obstruction of arterial circulation by neutral fat globules, followed by a delayed biochemical toxic injury caused by free fatty acids. The embolised small fat globules are deformable, and hence can traverse the capillary circulation of the lung even in the absence of a patent foramen ovale. Up to 60% of patients with CFE experience symptoms, and the condition is mostly self-limiting in nature, but recent studies have suggested that on the long term it may lead to neurocognitive impairment. The symptoms of CFE can vary considerably, typically appearing between 12 to 72 hours after the injury and can range from mild neurological symptoms to more severe symptoms like coma or even death in the most severe cases. There are no conclusive diagnostic tests or criteria developed for the diagnosis of FES making the diagnosis difficult. Frequently the diagnosis is based on a combination of symptoms, laboratory and imaging findings. Cerebral microbleeds (CMB) which can cause a differential diagnostic dilemma for CFE, have been in the centre of interest and target for many research publications in the past century, and has only recently gained even more attention due to the increase in neuroradiological imaging being performed on critically ill patients during the COVID-19 pandemic. Until today, there has not been any thorough investigation of cerebral microbleeds in relation to CFE, other than an increasing number of case reports describing these findings without raising their possible

significance. The criteria that have been proposed by Gurd and Wilson are currently the most commonly used diagnostic criteria. Many patients, however, do not experience the classic triad of cutaneous, respiratory and neurological symptoms. CFE have been revealed to be more common than previously anticipated by postmortem pathological studies, indicating that it is underdiagnosed, and the clinical criteria used to diagnose the condition are not entirely reliable. Neuroimaging has the potential to fill the gap between non-specific clinical symptoms and not entirely reliable criteria used for diagnosing CFE. Therefore, it is of utmost importance for the radiologist to actively seek lesions that might be associated with CFE in the appropriate clinical scenarios.

## 2. Objectives

1. We aimed to test our hypothesis through a systematic review of the literature according to which microbleeds show a characteristic pattern in CFE. This characteristic pattern could serve as diagnostic marker for CFE in the future.

2. We also aim to identify and evaluate the differential diagnostic possibilities of CFE that may be encountered by reporting radiologists. Through a review of the literature we intend to provide a better understanding of CFE and its differential diagnosis, contributing to more accurate and effective diagnosis, and ultimately leading to better patient outcomes.

By pursuing these two primary objectives, our research will provide critical insights into CFE diagnosis and differential diagnosis, potentially leading to improvements in clinical practice.

### 3. Methods

#### 3.1 Examining the cerebral microbleed characteristics in cerebral fat embolism

The first systematic review aims to test the hypothesis that microbleeds detected by MRI are common and show a characteristic pattern in cerebral fat embolism. We performed a systematic literature search, and a review of our local hospital records up to 31 January 2020. Patient data were individually scrutinised to extract epidemiological, clinical and imaging variables. Characteristic CFE microbleed pattern resembling a “walnut kernel” was defined as punctuate hypointensities of monotonous size, diffusely located in the subcortical white matter, the internal capsule and the corpus callosum, with mostly spared corona radiata and non-subcortical centrum semiovale, detected by susceptibility- or T2\* weighted imaging. The prevalence of this pattern and other, previously described MRI markers of CFE such as the starfield pattern and further diffusion abnormalities were recorded and statistically compared.

#### 3.2 Examining the differential diagnostic possibilities for cerebral microbleeds in cerebral fat embolism

In our second study, we investigated the imaging characteristics of the most common, and many of the rarely occurring possible mimickers of CMBs in CFE on SWI or T2\* images. We have searched the PubMed database up to 31 December 2022 for systematic review papers concentrating on the differential diagnosis of CMBs and their possible mimicking lesions. In the included literature, medical conditions directly associated with the presence of cerebral microbleeds detected on SWI or T2\* were collected. The MR susceptibility features of the mentioned conditions associated with CMBs were summarised and presented for each condition. MR susceptibility characteristics of the more rare conditions associated CMBs were not collected, as the number of cases did not allow for an accurate conclusion to be made as to the typical imaging features of CMBs in these conditions. The physiological

and physical background and possible ways of identification of microbleed mimics were summarised for each entity. Selected articles were qualitatively assessed, and no quantitative analysis was performed.

## 4. Results

### 4.1 Cerebral microbleeds in cerebral fat embolism

The literature search identified 277 articles, from which 193 articles were excluded, resulting in a total of 84 included articles. From the 84 included articles, there were 73 case reports, 6 review papers, 4 original papers, and 1 review pictorial essay. 140 patients from the included articles satisfied our inclusion criteria and were included in this review, in addition to the previously mentioned case from our own databases, resulting in an overall patient number of 141. In the included literature SWI was done in 40 cases, T2\* was performed in 21 cases, and both SWI and T2\* measurements were performed in 12 cases. Microbleeds in general, were present in 98.11%. The prevalence of the "walnut kernel microbleed pattern" was 89.74% (Figure 1). Diffusion abnormality in general, was seen in 97.64% of the cases. The starfield pattern description was used in 70.08% of the cases, but only 19.10% of these cases were confirmed with an ADC map (Figure 2).

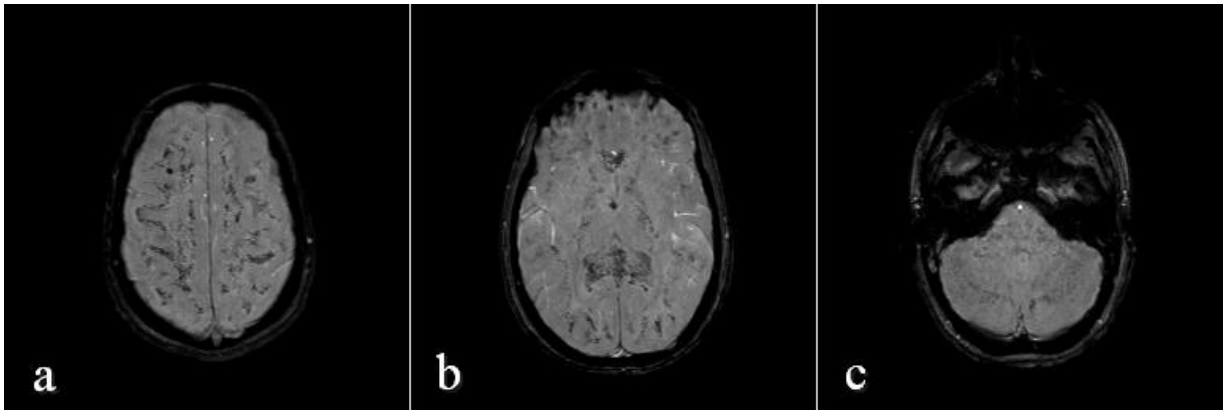


Figure 1 - SWI images of a 16-year-old female patient who suffered CFE a result of rib fractures and parenchymal abdominal organ injuries:

*a) at the level of the centrum semiovale, b) at the level of the basal ganglia and c) at the level of the posterior fossa. Diffuse, subcortical white matter, corpus callosum, brainstem and cerebellum punctiform hypointense SWI lesions characteristic of fat embolism are seen. Note that the corona radiata is mainly preserved (walnut kernel pattern) (a, b, c). On the right side, frontally, a drain has been inserted into the third ventricle (a, b)*

*Source: Department of Medical Imaging, University of Pécs Medical School.*

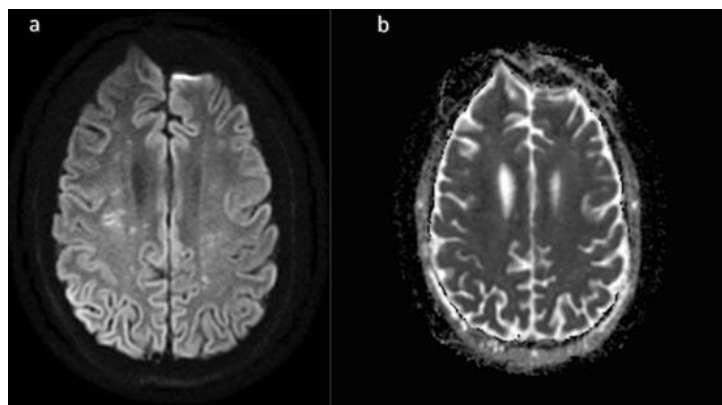


Figure 2 - A case representing the starfield pattern of restricted diffusion.

*MRI scan of an 18-year-old man with a closed displaced fracture of the left femoral shaft after a high velocity motor vehicle accident. Diffusion-weighted MR Image (TR/TE 10000/89 ms; b value, 1000 s/mm<sup>2</sup>) showing foci of hyperintensities within both centrum ovale (a), and the corresponding ADC map confirming restricted diffusion (b).*

Courtesy: G. Bierry and S. Kremer, Department of Radiology, University Hospital of Strasbourg, Strasbourg, France

The majority of the presented cases relied on T2 or DWI images only for using the starfield pattern term. A definitive starfield pattern was ascertained with images or accurate detailing of diffusion characteristics in the text in 68.5% of the cases. In 3.3% of the cases the term was used to describe foci of vasogenic edema, large confluent areas of cytotoxic edema, or infarcts on T2 images alone. Confluent restricted diffusion was seen in the corpus callosum in 77.27% of the cases. On follow-up studies brain atrophy has been confirmed in 9 cases. CFE related imaging findings are summarised in table 1.

Table 1 – Radiological findings

Variable	(n)	( $\Sigma$ ) *	Rate (%)
Microbleeds	52	53 <sup>1</sup>	98.11%
Walnut kernel microbleed pattern**	35	39 <sup>2</sup>	89.74%
Diffusion abnormality	124	127 <sup>3</sup>	97.64%
Definitive starfield pattern**	87	127 <sup>3</sup>	68.5%
Confluent cytotoxic edema in white matter	41	82 <sup>4</sup>	50%
Cytotoxic edema in the corpus callosum	34	44 <sup>5</sup>	77.27%
Vasogenic edema lesions	17	58 <sup>6</sup>	29.31%
Atrophy	9	9 <sup>7</sup>	100%

\*Total number of cases eligible for analysis \*\*for definition see methods <sup>1</sup> Cases with presented susceptibility- or T2\* images, or with no presented images but with clear description regarding microbleed presence. <sup>2</sup> Cases with susceptibility- or T2\* images in which the subcortical white matter, internal capsule, and the corpus callosum were evaluable, and cases with no presented images but description of findings

regarding microbleeds in the specified locations. <sup>3</sup> Cases with presented DWI, or DWI and ADC. Cases with no such presented imaging but with clear description of any diffusion abnormality, or the absence of any diffusion abnormality were also included. <sup>4</sup> Cases with presented DWI and ADC images. Cases without presented images but with description of findings regarding the presence or absence of confluent cytotoxic edema were also included. <sup>5</sup> Cases with DWI and ADC images where the corpus callosum is visible. Cases without presented images but with clear description regarding the presence or absence of corpus callosum diffusion restriction were also included. <sup>6</sup> Cases with presented DWI and ADC images. Cases without presented images but with clear description regarding the presence or absence of lesions of facilitated diffusion were also included. <sup>7</sup> Cases with presented follow-up MR or CT images. Cases without presented images but with clear description regarding the presence or absence of atrophy in the late stage.

Between the prevalence of the walnut kernel and definitive starfield patterns, the Fisher exact test showed a significant ( $p = 0.0073$ ) difference. In the subset of patients where both microbleed and starfield patterns were possible to be evaluated, the "walnut kernel pattern" prevalence was 93.1% of the cases, while the starfield pattern was present in 41.38% of the cases. The McNemar test showed these rates to be significantly different ( $p = 0.0003$ ). Regarding the temporal characteristics of the lesions (Figure 3), the starfield pattern was mostly present within the first 4 days after injury, while only positive in half of the cases in the 4-14 days period. On the other hand the walnut kernel microbleed pattern had a more consistent presence at all time points.

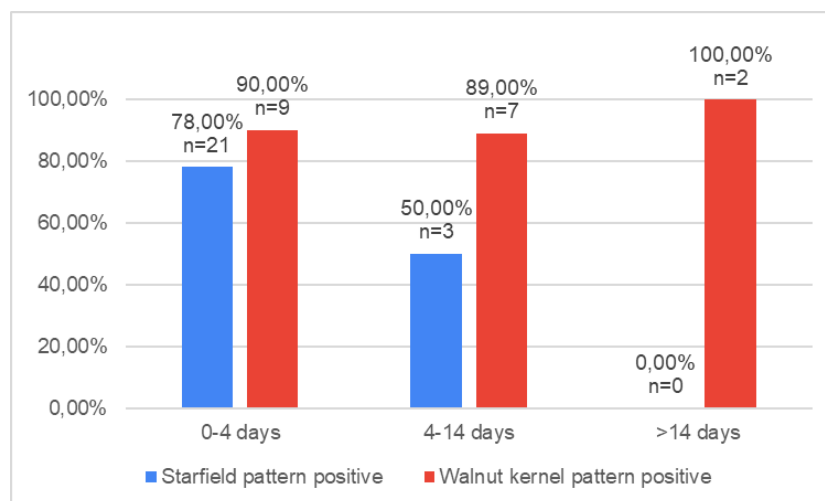
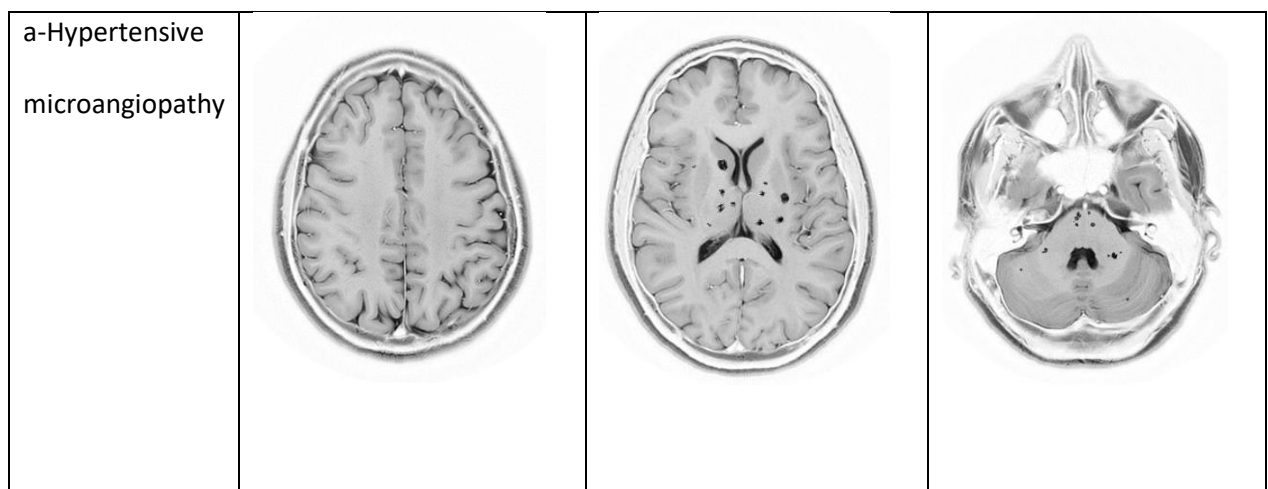


Figure 3 - Bar graph indicating the positive proportion of radiological patterns against time. *The starfield pattern was mostly present within the first 4 days after injury, while walnut kernel microbleed pattern had a more consistent presence among the different time periods.*



## 4.2 Cerebral microbleeds in medical imaging

The literature search identified 108 articles, from which 73 articles were excluded, resulting in a total of 35 included articles. In total 6 microbleed mimicking lesions that were found in the literature are microdissections, microaneurysms, microthrombi, microcalcifications, cavernomas and micrometastases. 10 categories of patients were found to be most commonly associated with cerebral microbleeds, and these were patients with no known medical conditions, patients with dementia and vasculopathy (including hypertensive), patients with chronic renal failure, patients with traumatic brain injury, patients who have previously underwent cerebral irradiation, patients who are critically ill, patients who underwent reperfusion therapies, and patients taking certain types of anti-thrombotic medications. A separate category was designated to other rare causes of cerebral microbleeds where we listed a total of 12 conditions that have been associated with CMBs in a smaller number of published cases in the literature (endocarditis, mountain sickness and acute respiratory failure, PRES, TTP, intravascular lymphomatosis or proliferative angioendotheliomatosis, moyamoya disease, sickle cell anemia/beta thalassemia, Fabry disease, Down syndrome, Parry–Romberg syndrome, and obstructive sleep apnea). Imaging features of the most commonly occurring entities are presented on a schematic drawing below (Figure 4).



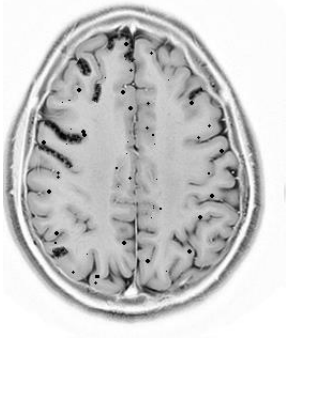
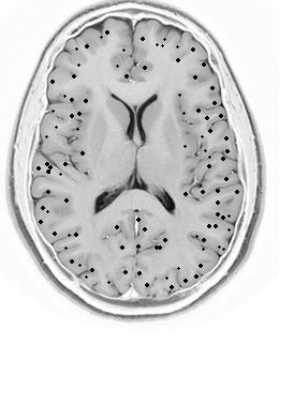
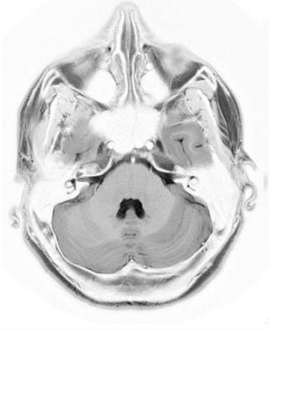
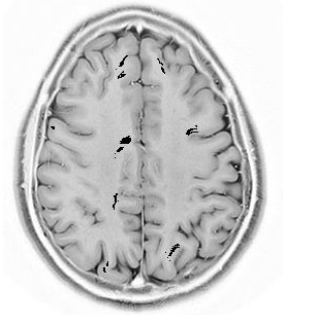
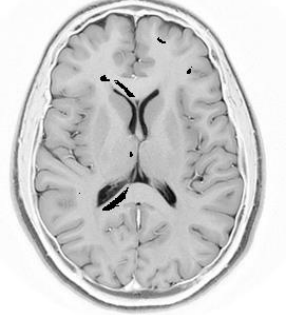
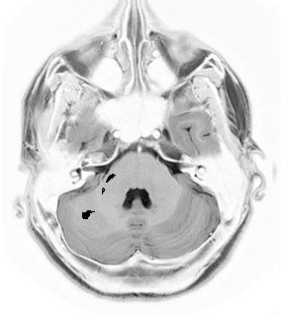
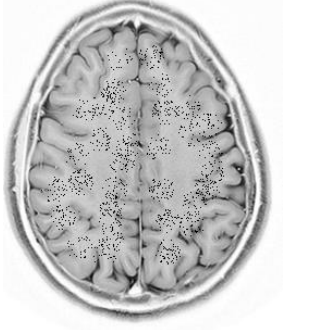

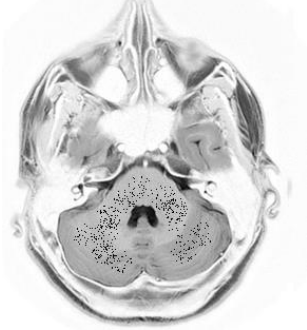
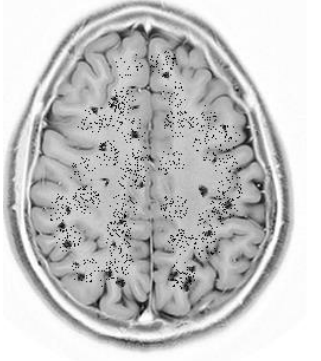
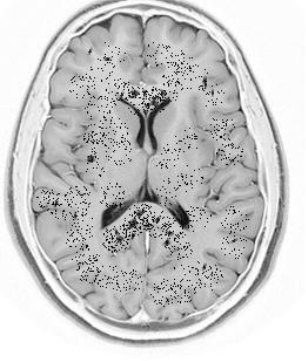
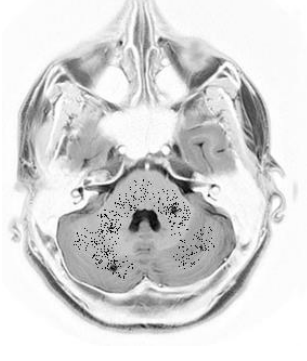
<p>b-Cerebral amyloid angiopathy</p>			
<p>c-Diffuse axonal injury</p>			
<p>d-Fat embolism</p>			
<p>e-Critically ill</p>			

Figure 4 – Schematic representation of cerebral microbleeds in in different conditions

*Schematic diagrams illustrating the appearance and distribution of CMBs in the most commonly occurring pathologies. (a) In hypertensive microangiopathy, CMBs can be seen in the area of the basal ganglia, pons, and cerebellar hemispheres. (b) In cerebral amyloid angiopathy, CMB can be seen at the gray-white matter interface with a lobar distribution (basal ganglia and pons are usually spared), superficial siderosis can also be seen as a trace of previous subarachnoid hemorrhage due to the involvement of the leptomeningeal vessels. (c) In diffuse axonal injury CMBs of varying size and morphology at the gray-white matter interface, in the corpus callosum and in the brainstem. (d) In fat embolism, we can see diffuse, subcortical white matter and punctate CMBs affecting the corpus callosum, while the corona radiata is mainly preserved (walnut kernel pattern). (e) In critically ill patients, diffuse involvement of the gray-white matter interface and the corpus callosum is typical, while deep and periventricular white matter and gray-matter remain spared (although the distribution is similar to that observed in fat embolism, but the size of CMBs are more heterogeneous).*

## 5. Discussion

Recognising and differentiating CFE from other conditions is important, as prompt diagnosis and initiation of supportive therapy improves the prognosis. The clinical diagnosis of CFE is often challenging, therefore imaging may have an added value in making a diagnosis and differential diagnosis. We hypothesized that the increasingly described microbleeds and their particular distribution, the walnut kernel pattern might be an important imaging marker for CFE. It can be noted that although the authors have previously not referred to this actual pattern of microbleeds, the walnut kernel pattern appears to be indeed very common in CFE, as it was present in 89.74% of the cases. Recognizing this specific pattern could be of utmost importance because CMBs in other

distributions can be associated with a number of other, possibly coinciding pathologies such as diffuse axonal injury (DAI), sepsis, hypertension, amyloid angiopathy amongst others. In certain conditions, such as in the critically ill (sepsis, COVID-19), or in cases where patients receive extracorporeal membrane oxygenation can have a quite similar microbleed lesion morphology and distribution to the walnut kernel pattern, therefore it is very important for radiologist to be informed whether the patient undergone such therapy, but the lesions in these conditions tend to be more variable in size. The exact pathomechanism of cerebral microbleeds in the critically-ill in general and in patients undergoing ECMO therapy is not known, but our research group speculates that the underlying pathomechanism could be similar to that of CFE. Further imaging research and accompanying post-mortem studies might elucidate differential diagnosis and the exact mechanisms of microbleeds in critically ill patients. Beyond microbleeds several types of CFE MR signs have been described in previous studies. Amongst which the starfield pattern is the most widely known radiological sign. Our published review revealed a very similar occurrence rate 68.5% of the starfield pattern in CFE to that published in the literature. However, the more recent papers included considerably more SWI and T2\* studies, revealed that microbleeds, and specifically the walnut kernel pattern may be even more common than the starfield pattern. An emerging concern regarding the starfield pattern is that it has been extensively used in the literature without considering the ADC values. According to our findings this was the case in around half of the reviewed patients. From a practical point of view, it is important to note that compared to the starfield pattern, over time, microbleeds could be more consistently identified on MRI. The starfield pattern is typically present in the first 4 days, whereas in the 4–14 day time interval the number of positive and negative cases are equal. In contrast, irrespective of the time point, microbleeds were always more commonly present than absent—indicating constant visibility (Figure 3). An additional remarkable observation of our review is that the previously described “confluent cytotoxic edema” is mostly present in the corpus callosum, with a prevalence of 77.27%, which is comparable to the starfield and walnut kernel patterns. There is limited data in the literature regarding

the chronic radiological sequel of CFE, cerebral atrophy and persistent T2 hyperintensities has been described in some cases.

Our study has certain limitations. First, comparison for the rates of the starfield and walnut kernel patterns is somewhat limited, since considerably more studies have investigated diffusion abnormalities than microbleeds. Second, the prevalence of the investigated imaging patterns do not necessarily reflect their true sensitivity, since it is possible that authors published their imaging results more likely in case of positive findings, causing seemingly higher prevalence of these imaging markers. Third, data regarding chronic changes induced by CFE are scarce and therefore the prevalence of cerebral atrophy remains unknown. Still, it can be safely postulated that the walnut kernel microbleed pattern, the starfield pattern and corpus callosum diffusion restriction are the most common imaging alterations in CFE, and can be regarded as a reliable imaging markers of CFE.

## 6. Novel findings and conclusion

- a. We managed to identify an imaging marker (walnut kernel microbleed pattern) related to CFE, which was not considered in any scientific work previously.
- b. We have proven that microbleeds in this detailed constellation are more characteristic markers of CFE than any other known imaging feature.
- c. We found that the walnut kernel microbleed pattern together with the other known imaging features, CFE can be confidently diagnosed in all stages of the condition.
- d. We have identified the possible mimicking entities of CFE, thus our work provides a practical aid to the clinical and radiological diagnosis of CFE.

Due to the unforeseeable pandemic in the past three years, our work has gained much significance, as with the increasing amount of the critically ill patients treated in hospitals, CFE cases has shown an unprecedented increase in number. This is reflected by the fact that number of publications listed on PubMed with the terms “cerebral microbleeds”, and “cerebral fat embolism” has been showing a steady increase since 2018. Providing the clinicians with a reliable diagnostic marker for CFE is currently invaluable.

CFE is rare but potentially life threatening condition and its clinical presentation can be dramatic. However, despite the severity of the symptoms, prompt diagnosis and initiation of supportive therapy often improves the prognosis. Therefore it is crucial for medical professionals, including radiologists to be aware of and recognise this condition in order for them to consider it in the appropriate clinical scenarios.

## 7. List of publications

### 7.1 Publications related to the current work

- Giyab O, Balogh B, Bogner P, Gergely O, Tóth A. Microbleeds show a characteristic distribution in cerebral fat embolism. *Insights Imaging*. 2021 Mar 31;12(1):42. doi: 10.1186/s13244-021-00988-6. PMID: 33788069; PMCID: PMC8010501. IF 5.964 Q1 (2021)

- Giyab O, Balogh B, Bogner P, Gergely O, Tóth A. Agyi mikroszkopikus vérzések differenciáldiagnosztikája. *Magyar Radiológia Online*. 2022. Sep ;13(3): 1.

### 7.2 Other publications

- Orsi G, Cseh T, Hayden Z, Perlaki G, Nagy SA, Giyab O, Olsen DA, Madsen JS, Berki T, Illes Z. Microstructural and functional brain abnormalities in multiple sclerosis predicted by osteopontin and neurofilament light. *Mult Scler Relat Disord*. 2021 Jun;51:102923. doi: 10.1016/j.msard.2021.102923. Epub 2021 Mar 24. PMID: 33813096. IF 4.808, Q1 (2021)

- Molnár K, Kálmán E, Hári Z, Giyab O, Gáspár T, Rucz K, Bogner P, Tóth A. False-Positive Malignant Diagnosis of Nodule Mimicking Lesions by Computer-Aided Thyroid Nodule Analysis in Clinical Ultrasonography Practice. *Diagnostics (Basel)*. 2020 Jun 6;10(6):378. doi: 10.3390/diagnostics10060378. PMID: 32517227; PMCID: PMC7345888. 5 year IF 4.129, IF 3.706, Q2 (2020)

- Szuper K, Giyab O, Than P. Térközeli lateralis cystosus elváltozások differenciáldiagnosztikája [Differential diagnosis of lateral cystic lesions in the knee joint]. *Orv Hetil*. 2019 Apr;160(15):593-599. Hungarian. doi: 10.1556/650.2019.31325. PMID: 30957539. IF 0.615, Q4 (2019)

- Weninger C, Várady E, Omar G, Szabó I, Tornóczky T. A case of primary leiomyosarcoma originating from the inferior vena cava. *Orvosi Hetilap*. 2019 May 1;160(19):756-61. IF 0.615, Q4 (2019)

- Weninger C, Dérczy K, Giyab O, Schmidt E, Szabó Z, Szekeres S, Sarkadi M, Zámbó K. Possibility of SPECT/CT in examination of endocrine diseases. European Congress of Radiology-ECR 2015.
- Jaray A, Giyab O, Harmat Z, Battyany I. Proper settings of technical parameters in contrast enhanced ultrasound examinations to avoid pitfalls and artifacts-tips and tricks. European Congress of Radiology-ECR 2012.
- Imaging of Non-alcoholic Fatty Liver Disease / Chapter 4. Zoltán Harmat , Omar Giyab, ISBN 978-1-68108-466-4 First published in 2017

### 7.3 Scientific presentations related to the current work

- European Congress of Radiology 2022 overture research presentation titled “Microbleeds in cerebral fat embolism” #12749. 2.-6. March 2022
- Hungarian congress of neuroradiology – The differential diagnosis of cerebral microbleeds. 3.-6. November 2021
- Slovak - Croatian - Hungarian - Slovenian Radiological Symposium - The role of SWI in the detection of cerebral fat embolism. 15-17. March 2019
- 19. Pécsi Intervenció Radiológiai Szimpózium – The possible role of SWI in the diagnosis of cerebral fat embolism. 25. October. 2018



## 8. Acknowledgements

I would like to express my deep gratitude and appreciation to everyone who has supported me throughout my journey. First and foremost, I want to thank my family for their constant love and encouragement. My wife Eliza and son Naszim have been my pillars of strength. Eliza has always been there to provide me with the support and motivation I needed at every moment to complete this journey.

I would also like to extend my heartfelt gratitude to my parents for their unwavering support and belief in me. Their guidance and encouragement have been instrumental in shaping me into the person I am today.

I am thankful to my tutors, Dr. Arnold Tóth and Dr. Gergely Orsi, for their invaluable guidance, and encouragement throughout my research work. I am especially indebted to my tutor and friend Dr. Tóth, whose mentorship, unwavering support and commitment to my research have been instrumental in helping me to complete every step of this journey. His expertise and insights have been invaluable, and I have learned so much under his guidance.

I would also like to express my gratitude to my colleague Dr. Andrea Horváth, whose guidance in finalizing this Ph.D. booklet were invaluable.

Finally, I would like to express my sincere appreciation to the Head of the Department, Professor Péter Bogner, for his encouragement and support throughout my research work. His valuable feedback and encouragement have been instrumental in shaping my work, and I am deeply grateful for his mentorship.

Once again, I would like to thank everyone who has contributed to my success in any way and helped me achieve my goals.